Quantification and reduction of attenuation related artifacts in SPET by applying attenuation model during iterative image reconstruction: A Monte Carlo study

Faraz Kalantari[1] PhD,
Hossein Rajabi[1] PhD,
Mohsen Saghari[2] MD

1. Department of Medical Physics, Faculty of Medical Sciences, Tarbiat Modares University, Tehran, Iran
2. Research Institute for Nuclear Medicine, Tehran University of Medical Sciences, Tehran, Iran

***

Keywords: SPET - Artifact - Attenuation correction - OSEM - Monte Carlo simulation

Correspondence address:
Hossein Rajabi PhD
Department of Medical Physics, Faculty of Medical Sciences, Tarbiat Modares University, Tehran, Iran
P.O. Box 14115-331,
Tel: +98-21-82883894,
Fax: +98-21-88006544,
E-mail: hrajabi@modares.ac.ir

Received:
11 May 2011
Accepted revised:
8 July 2011

Abstract

Photon attenuation is one of the main causes of the quantitative errors and artifacts in SPET. A transmission or CT based attenuation map is necessary to correct for the effects of attenuation accurately. *In this research*, some important attenuation related artifacts are described. A fast and memory efficient iterative algorithm is proposed for attenuation correction. Ordered subset expectation maximization (OSEM) algorithm with attenuation model was applied for image reconstruction. Monte Carlo simulation was used to create the projections in this study. Different voxel based phantoms with uniform and non-uniform activity distributions and attenuation maps were employed to evaluate the accuracy of this algorithm. The NCAT digital phantom was also used to investigate the attenuation effects on myocardial perfusion SPET in men and women. Projections free from the effect of attenuation were also simulated. The reconstructed image from these attenuation-free projections was considered as reference image. Our attenuation correction algorithm was evaluated by its ability to recover activity and to remove attenuation related artifacts. *The mean-square-error (MSE) between* reference and corrected image and image contrast were calculated for quantitative evaluation of this algorithm. A variety of attenuation related artifacts were observed. Moreover anterior wall of myocardial perfusion images of female phantom and inferior wall in male phantom were affected by attenuation. All of the attenuation related artifacts were removed after attenuation correction. Quantitatively, the MSE values between reference images and corrected images were reduced by about 900% for all phantoms. *In conclusion*, by applying our new method for incorporating attenuation model during OSEM, we were able to eliminate a variety of artifacts and errors, which is a necessary step for quantitative SPET.

Hell J Nucl Med 2011; 14(3): 278-283 *Published on line: 10 November 2011*

Introduction

The main objective of single photon emission tomography (SPET) is determining the activity distribution inside the patient's body. To achieve this goal, a rotating gamma camera acquires a large number of projections around the patients. Reconstruction algorithms are used to convert the projections into three-dimensional images. To a first approximation, a pixel value in a projection is the ray sum of the activities in a column in front of it. Hence, projections are considered the Radon transform of the activity distribution inside the patients' body [1-3]. This suggests inverse Radon transform and its numerical implementation, filtered back projection (FBP), as the prime method for image reconstruction [3, 4]. However, in this assumption, the attenuation of photons inside the objects is ignored [2, 3]. Therefore a variety of attenuation related artifacts are introduced in the final reconstructed image.

In order to compensate for the attenuation in FBP reconstruction, data should be corrected before or after reconstruction. The main problem in correcting data before reconstruction is determining the compensation required for each pixel of the projections. There are limited studies that introduced approximate methods for attenuation correction before reconstruction [5]. Application of these methods is still limited to uniform activity distribution inside uniform attenuating media. Applying the attenuation correction on reconstructed image rectifies the limitation on activity distribution; but it is still limited to uniform attenuation media [6]. This method is suitable for SPET imaging of the brain because it has almost similar attenuation properties at all directions [7]. There are also techniques to correct the reconstructed images for non-uniform attenuating media [7-10]; but, at the cost of noise amplification, particularly in the center of objects that is usually more affected by attenuation.

Iterative reconstruction methods are better suited to correction of the physics of imaging, including attenuation. These algorithms provide the possibility to use more realistic

models for generation of mathematical projections that may lead to more realistic reconstructed images [11-15]. The most commonly used iterative method in SPET is maximum likelihood expectation maximization (MLEM) [16, 17]. Nowadays, ordered-subsets expectation maximization (OSEM) that is a fast implementation of MLEM is commonly used [18]. In this research we introduced a novel approach for incorporating attenuation map during OSEM. This method employs a rotating image in a fix grid to create attenuated projections from each estimate and to back project the error from each angle. Therefore we avoided saving the huge imaging matrix for attenuation modelling.

There are only limited studies that describe attenuation related artifacts in SPET. In this paper we assessed SPET attenuation related artifacts and quantitative errors associated with the attenuation. We applied our fast and memory efficient method for attenuation correction during iterative reconstruction algorithms. Finally the value and importance of attenuation correction was evaluated on a variety of phantom configurations.

Methods

Digital phantoms

The digital phantoms employed herein with Monte Carlo simulation consist of two parts, the attenuation map and the activity distribution map. We used four types of phantom in this investigation.

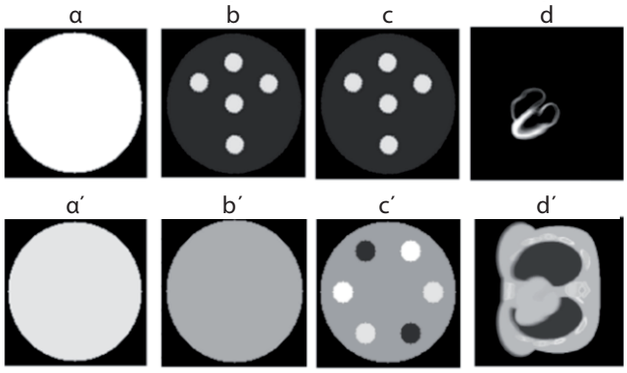

Figure 1. The digital phantoms used in this study were composed of activity distribution map and their corresponding attenuation map (bottom raw).

A single slice uniform medium (water equivalent μ=0.149cm^{-1}) as the attenuation map (Fig. 1-a) and a similar size (40X40cm) uniform metastable technetium-99 (^{99m}Tc) source as activity distribution map (Fig.1-a′). Phantom was digitized into 128X128 voxels of 0.3125X0.3125cm. This phantom was used to investigate the hot skin artifact. A single slice uniform medium (water equivalent μ=0.149cm^{-1}) was used as attenuation map (Fig. 1-b) and a similar size phantom containing five circle shape disk of ^{99m}Tc (40X40cm) in cold background (activity-to-background ratio 5:1) as activity distribution map (Fig. 1-b′). This phantom was used for quantitative evaluation of the results. The dimensions and its resolution were similar to the first phantom.

A similar size, single slice uniform medium was used (water equivalent μ=0.149cm^{-1}) containing six circle shape disks of different attenuation properties, (lungs, μ=0.043cm^{-1}; rib bone, μ=0.219cm^{-1} and skull bone, μ=0.242cm^{-1}) representing an extremely nonuniform media (Fig. 1-c). A similar size phantom containing five circle shape disk of ^{99m}Tc (hot spot) in cold background (activity-to-background ratio 5:1) was used as activity distribution map (Fig. 1-c′).

To evaluate the overall performance of attenuation correction in a realistic condition, the nonuniform B-spline (NURBS) based cardiac torso (NCAT) phantom was used [19]. This phantom has been derived from computed tomography (CT) images of human and precisely models the torso organs. To evaluate breast attenuation artifacts, a typical female body torso was generated. A typical male torso was also generated to assess diaphragmatic attenuation effect in men. The NCAT phantom produces the attenuation map and the activity distribution map automatically based on the user defined data. In activity distribution map (Fig. 1-d), ^{99m}Tc activity was considered in myocardium, liver, spleen and other parts of torso (myocardium: liver: spleen: lung: background 100: 40: 22: 6: 6) based on published data for methoxyisobutyl isonitrile (MIBI) bio-distribution [20, 21]. The corresponding attenuation map was created at photon energy of 140keV (Fig.1-d′). The phantom dimension was 40X40X20 and digitized into 128X128X64 voxel arrays.

Monte Carlo simulation

The Monte Carlo code, SIMIND version 49, was used to image the phantoms [22]. A typical SPET system (Argus, ADAC, USA) with low energy high resolution (LEHR) collimator, 3.4mm intrinsic spatial resolution, 9.7% energy resolution (at 140keV) was modeled in this study. A total number of 128 projections at 128 x128 matrix size were acquired in 360 degrees around the phantoms (radius of rotation=30cm); however for NCAT cardiac phantom, simulation was done at 180 degrees from right anterior oblique (RAO) to left posterior oblique (LPO) to model a real cardiac SPET. Since scatter correction was not aimed in this study, only primary photons were considered to form the projections. One million photon histories per projection were traced. As a reference image, an attenuation free image from each activity phantom (in air) was also generated.

Image reconstruction

All of the SPET images were reconstructed using both FBP and iterative OSEM reconstruction methods. The FBP reconstruction included a Hanning filter with a 0.7 Nyquist cutoff frequency. The SPET data were also reconstructed using the OSEM algorithm with and without attenuation correction. It is well known that the signal to noise ratio (SNR) characteristics (and therefore the uniformity) of the images reconstructed with OSEM change as a function of iteration number. To make a reasonably fair comparison between the results from FBP versus those from OSEM, the OSEM images were reconstructed using the number of iterations that produced images that most closely matched the SNR characteristics of those reconstructed using FBP. The SNR was assessed quantitatively by dividing the mean of pixel values as signal and the standard deviation of pixel values as noise on a region of interest (ROI) that contained 1.256 pixels within the uniformity phantom. Number of subsets was 8 for OSEM algorithm throughout this research. This means 16 angles per subset for 360 degrees and 8 angles per subset for 180 degrees SPET.

Attenuation correction algorithm

To correct for the effect of attenuation, a pair of attenuated projection/backprojection was used during OSEM. A rotating image in a fix grid was used to create forward projections from each estimate and to back project the error from each angle. Bilinear interpolation was applied to refine the rotated image for each angle.

Attenuation phantom was blurred with a Gaussian kernel to equate its resolution with the emission images [23, 24]. This blurred image simulates a CT image which filled by linear attenuation coefficients. Using this attenuation map, in each angle, attenuation factor (AF) was calculated for each pixel as:

$$AF(i,j)=\frac{I}{I_0}=EXP\left(-d\left(\sum_{k=j+1}^{\infty}\mu(i,k)+\frac{1}{2}\mu(i,j)\right)\right) \quad \text{(Eq. 1)}$$

Where d stands for pixel width and is a fixed value because the grid is always fixed with columns parallel to detector face. I_0 and I are the number of emitted and the number of detected photons respectively. For each pixel located at (i,j), the amount of AF can be calculated by exponential of the sum of attenuation coefficients from that pixel to the end at direction of perpendicular to the camera multiplied by d. The value of one-half the pixel dimension is usually used as an approximation for the self-attenuation in the source voxel. The AF matrix is multiplied by estimated image. Projection of the result matrix is then calculated as a simple ray sum of the pixels at that angle. This results in attenuated projection. After comparing this mathematical projection with corresponding actual projection, the error was backprojected into error matrix from that angle. This final error matrix was calculated by multiplication of error matrix by AF matrix as well to consider the effect of attenuation in backprojection.

For next projection both attenuation map and estimated image were rotated in their fixed grids. Once again AF matrix was calculated and multiplied by rotated image and projection was calculated for this new angle (Fig. 2). At the same time, the error matrix was also rotated in a fix grid to be ready for backprojecting error from this new angle. This procedure was repeated until all projections were enrolled for filling error matrix. The new estimate was calculated by simple multiplication of error matrix by current estimate. Since attenuation was modeled in forward projection, a better and more realistic comparison was done; therefore the final reconstructed image tended to be free from attenuation effect.

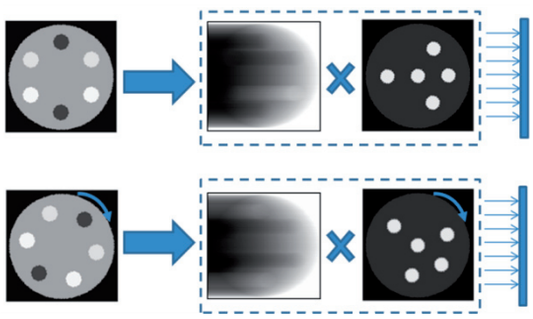

Figure 2. Creating attenuated projections from an estimated image in two different angles.

Evaluation parameters

Mean pixel value in same size circular regions of interest (ROI), contrast and normalized mean square error (NMSE) were calculated to evaluate the results. Contrast was calculated as the ratio of difference to sum of the mean pixel values in hot and cold regions. To evaluate the amount of similarity between each reconstructed image (I) and reference image (I_0), MSE was calculated as:

$$MSE=\sqrt{\frac{\sum_{i,j=1}^{n}(I_0(i,j)-I(i,j))^2}{n\times n}} \quad \text{(Eq. 2)}$$

This value was then scaled to be a number between 0 and 1. This helped to evaluate relative variation of similarity between reference image and images before and after correction. We called this value as NMSE.

Results

Figure 3 shows the SNR versus iteration number for the SPET images obtained from the uniform disk phantom. The SNR obtained from FBP is plotted as a constant value (i.e., independent of iteration number) and produces a SNR similar to that obtained with OSEM at iteration 8 when the image was reconstructed using the OSEM method without any corrections and iteration 9 when reconstructed using the OSEM method with attenuation correction. On the basis of this result, 9 iterations to reconstruct SPET data of phantoms and patients imaged were used throughout this article.

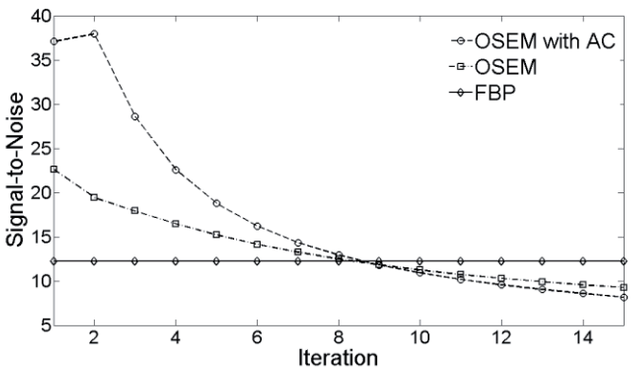

Figure 3. SNRs against iteration number for images reconstructed with FBP, OSEM without attenuation correction, and OSEM with attenuation correction.

For each phantom configuration, results were compared according to mean pixel values, relative contrast and normalized mean square error (NMSE). Both corrected and non-corrected images were compared with reference image that acquired in air without any attenuation.

a) Uniform activity in uniform attenuation phantom

Hot skin artifact is seen in Figure 4(a) and (b) as one of the most famous attenuation related artifacts [25]. As shown in Figure 4(c), this artifact has been removed after attenuation correction. This result is comparable with our reference attenuation free image (Figure 4(d)). Pixel values along a line profile passing from the center of each image have been shown in Figure 4(e).

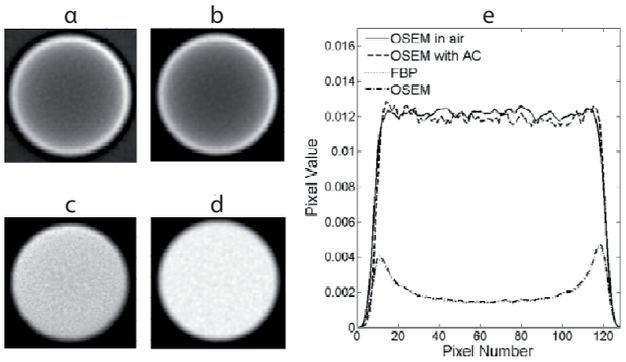

Figure 4. Reconstructed images: a) without AC using FBP, b) without AC by OSEM, c) after AC by suggested algorithm, d) reference attenuation free image e) Pixel values along a vertical line profile passing from the center of each reconstructed image.

b) Non-uniform activity in uniform attenuation phantom

As shown in Figure 5(a) and (b) attenuation causes both hot skin artifact and contrast reduction for the central hot circle (central spot). Mean pixel values in central spot, circles placed near the skin (edge spots) and background were used to calculate the contrast. As shown in Table 1 the contrasts for the edge spots are almost the same before and after attenuation correction. On the other side, there is a considerable reduction in contrast for the central spot which results inaccurate quantitative and qualitative assessments. This artifact in addition to hot skin artifact has been removed after attenuation correction as shown in Figure 5(c). The value of NMSE was also reduced from 1 in non-corrected OSEM image to 0.071 in corrected image.

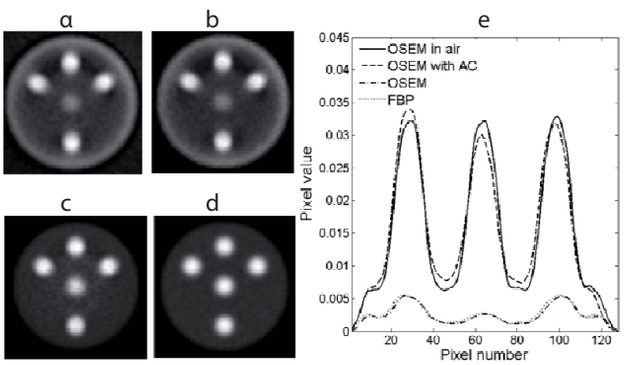

Figure 5. Reconstructed images of five hot circles (spots) in uniform water cylinder: a) without AC by FBP, b) without AC by OSEM, c) after AC by suggested algorithm, d) reference attenuation free image, e) Pixel values along a vertical line profile passing from the center of each reconstructed image.

c) Non-uniform activity in non-uniform attenuation phantom

There are many artifacts associated with this phantom configuration. As shown in Figure 6(a) and (b), two bright spots are shown in places that there were lung equivalent materials in the attenuation phantom. The contrast associated with these bright artifacts is comparable with contrast of central hot spot. This artifact can cause inaccurate interpretation. As shown in Figure 6(a) and (b), it seems that there are three low contrast hot spots along the diagonal direction of non-corrected images. There are also four artificial cold spots in places that there were bone equivalent materials. Moreover, hot skin artifact and low contrast central spot artifact also exist. All artifacts are almost removed after attenuation correction (Fig. 6(c)). The value of NMSE was also reduced from 1 in the non-corrected OSEM image to 0.063 in the corrected image. Considerable enhancement in contrast of central spot was also observed after attenuation correction.

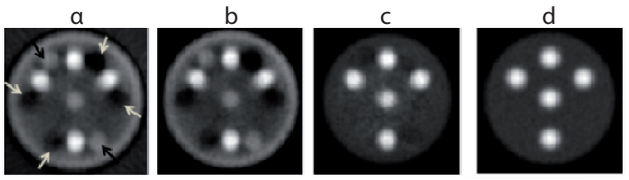

Figure 6. Reconstructed images of five hot spots in non-uniform attenuating cylinder: a) without AC by FBP, lung related bright spot artifacts (black arrows) and bone related cold spot artifacts (white arrows) b) without AC by OSEM, c) after AC by suggested algorithm, d) reference attenuation free image.

d) NCAT torso phantom

Compared to the attenuation free images, there were many attenuation related artifacts in attenuated image. These artifacts were mainly false positive defects in the inferoseptal and the anterior wall of myocardium (Fig. 7) in female phantom and false positive defects in the inferoseptal and the inferior wall of myocardium (Fig. 8) in male phantom. Moreover, lung related bright spots and bone related cold spots (Fig. 9a and b) can affect qualitative interpretations. All artifacts are almost removed after attenuation correction (Fig. 9c). Quantitatively, NMSE was reduced from 1 in the non-corrected OSEM image to 0.10 in the corrected image. According to Figure 9e, a much better fits between the pixel values of reference image and the corrected image were found in comparison with non-corrected images. Left ventricle to background activity also increased from 0.67 in the non-corrected image to 0.79 in the corrected image.

Table 1. *Mean pixel values and contrasts for non-uniform activity and uniform attenuation*

Parts of images	Edge spots NAC	Edge spot AC	Center spot NAC	Center spot AC
Mean pixel value	0.0051	0.030	0.0025	0.027
Spot to background contrast	0.62	0.61	0.35	0.57

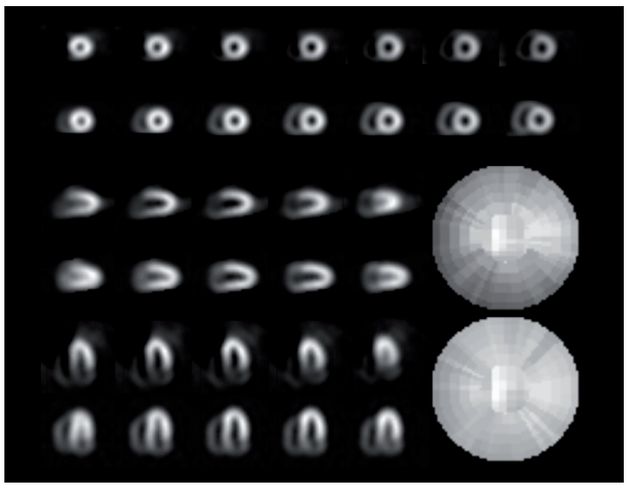

Figure 7. Reconstructed images of NCAT female phantom by FBP. Without AC (top rows). Reference attenuation free image (bottom rows), from three standard views and their corresponding bull's eye plots

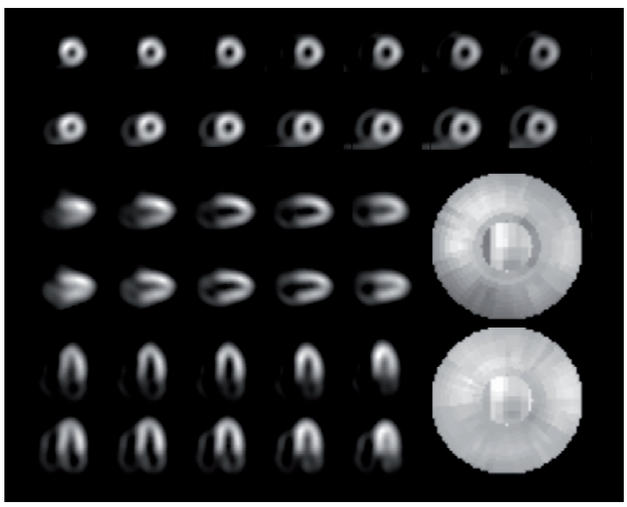

Figure 8. Reconstructed images of NCAT male phantom by FBP. Without AC (top rows). Reference attenuation free image (bottom rows), from three standard views and their corresponding bull's eye plots

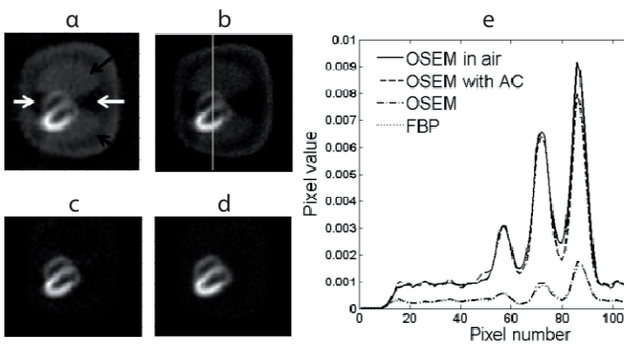

Figure 9. A transverse slice of reconstructed image of the NCAT phantom: a) without AC by FBP, lung related bright spot artifacts (black arrows), bone related cold spot artifacts (white arrows) and loss of activity in septal wall due to the attenuation, b) without AC by OSEM, c) after AC, d) reference attenuation free image, e) Pixel values along a vertical line shown in b for each reconstructed image.

All above artifacts were completely removed by our correction algorithm. A considerable increase in amount of activity was achieved after attenuation correction. The value of NMSE that represents the error between reference image and corrected image was reduced by about 900%.

Discussion

In this paper we reviewed the attenuation related artifacts and suggested a novel anatomical based attenuation correction algorithm for both uniform and non-uniform objects.

Hot skin artifact as the most obvious effect of attenuation was shown in all phantom configurations. Contrast degradation in central hot spot was another obvious attenuation related artifact. This artifact happens even in uniform objects like brain and must be compensated to avoid the errors associated with quantitative and qualitative image interpretation. By contrast central hot spots, edge spot contrasts were not affected by attenuation. This artifact shows that activity reduction inside an object doesn't follow a linear process. For cases in which the attenuating medium was nonuniform, non-uniformities were introduced into the final reconstructed image. The most notable example was in the lungs, as shown in Figures 6 and 9. For non-uniform objects, the lung related bright spots and bone related cold spots were shown as two major artifacts.

Nonhomogeneous photon attenuation in the thorax is one of the most notable limitations of myocardial perfusion imaging. By focusing on myocardial perfusion, some false positive results were observed. This is in agreement with many clinical trials demonstrated that attenuation correction can significantly increase specificity (or normalcy rate) in myocardial SPET [26, 27].

The advantage of using Monte Carlo simulation is that we are aware about our input phantoms and we can control all effective parameters in imaging procedure. For example we create attenuation free projections as our reference image and we neglect scatter photons in this study which are not possible in practice. However there are some limitations that should be considered using this algorithm in practice. This algorithm works well when we have projections free of scatter photons. It is therefore necessary to recognize and remove scattered photons either before reconstruction for example by using dual or triple energy windows [28-30] or during reconstruction by modeling these photons in iterative methods [16, 31].

In this study we used attenuation phantom as our attenuation map. Therefore we had a noise free map with perfect registration. In clinical practice however, we don't have such attenuation map and it should be acquired using either external source or CT [32-34]. Nevertheless, there are always some drawbacks in the attenuation map. One of the main problems is the error associated by misalignment between emission and transmission image which poses the risk of incomplete correction and thus artificial perfusion defects. Especially in myocardial SPET/CT that transmission data are usually acquired in a very shorter time compared to emission data associated with respiratory or other voluntary motions [35, 36].

In this research we simulated high count projections which results in very good signal to noise ratio. In clinical practice however, acquiring these projections is not practical or time consuming for each patient which makes it not practical. It has been shown that when we consider degrading factors like attenuation in iterative methods, usually a higher number of iterations should be used to reach artifact free images [17]. On the other hand, when the number of iterations rises up, SNR of reconstructed image will decrease. Therefore a compromise should be made between statistical noise and artifacts in real clinical images.

In conclusion, our study suggests that by using our new method for incorporating attenuation model during OSEM, it is possible to eliminate a variety of artifacts and errors, which is a necessary step for quantitative SPET.

Acknowledgements
The authors would like to thank professor Michael King, Department of Radiology, Division of Nuclear Medicine, University of Massachusetts Medical School, for his valuable comments on this manuscript.

The authors declare that they have no conflicts of interest.

Bibliography

1. Radon J. On the determination of functions from their integrals along certain manifolds. *Math Phys Klass* 1917; 69: 262-77.
2. Bruyant PP. Analytic and Iterative Reconstruction Algorithms in SPECT. *J Nucl Med* 2002; 43: 1343-58.
3. Zaidi H. Quantitative analysis in nuclear medicine imaging. New York: Springer Science Business Media, Inc; 2006; 82-106.
4. Hutton BF, Hudson HM, Beekman FJ. A clinical perspective of accelerated statistical reconstruction. *Eur J Nucl Med* 1997; 24: 797-808.
5. Jaszczak RJ, Murphy PH, Huard D, Burdine JA. Radionuclide emission computed tomography of the head with 99m Tc and a scintillation camera. *J Nucl Med* 1977; 18: 373-80.
6. Chang LT. A method for attenuation correction in radionuclide computed tomography. *IEEE Trans Nucl Sci* 1978; 25: 638-43.
7. Arlig A, Gustafsson A, Jacobsson L et al. Attenuation correction in quantitative SPECT of cerebral blood flow: a Monte Carlo study. *Phys Med Biol* 2000; 45: 3847-59.
8. Fleming JS. A technique for using CT images in attenuation correction and quantification in SPECT. *Nucl Med Commun* 1989; 10: 83-97.
9. Ljungberg M, Strand SE. Attenuation correction in SPECT based on transmission studies and Monte Carlo simulations of build-up functions. *J Nucl Med* 1990; 31: 493-500.
10. Ljungberg M, Strand SE. Attenuation and scatter correction in SPECT for sources in a nonhomogeneous object: a monte Carlo study. *J Nucl Med* 1991; 32: 1278-84.
11. Gullberg GT, Huesman RH, Malko JA et al. An attenuated projector-backprojector for iterative SPECT reconstruction. *Phys Med Biol* 1985; 30: 799-816.
12. Tsui BMW, Hu H-B, Gilland DR, Gullberg GT. Implementation of Simultaneous Attenuation and Detector Response Correction in SPECT. *IEEE Trans Nucl Sci* 1988; 35: 778-83.
13. Zeng GL, Gullberg GT. Three-Dimensinal Iterative Reconstruction Algorithms with Attenuation And Geometric Point Response Correction. *IEEE Trans Nucl Sci* 1991; 38: 693-702.
14. Beekman FJ, den Harder JM, Viergever MA, van Rijk PP. SPECT scatter modelling in non-uniform attenuating objects. *Phys Med Biol* 1997; 42: 1133-42.
15. Seo Y, Wong KH, Sun M et al. Correction of photon attenuation and collimator response for a body-contouring SPECT/CT imaging system. *J Nucl Med* 2005; 46: 868-77.
16. Shepp LA, Vardi Y. Maximum Likelihood Reconstruction for Emission Tomography. *IEEE Trans Med Imaging* 1982; 1: 113-22.
17. Lange K, Carson R. EM reconstruction algorithms for emission and transmission tomography. *J Comput Assist Tomography* 1984; 8: 306-16.
18. Hudson HM, Larkin RS. Accelerated Image Reconstruction using Ordered Subsets of Projection Data. *IEEE Trans Med Imag* 1994; 13: 601-9.
19. Segars WP, Lalush DS, Tsui BMW. Modeling respiratory mechanics in the MCAT and spline-based MCAT phantoms. *IEEE Trans Nucl Sci* 2001; 48: 89-97.
20. El-Ali HH, Palmer J, Carlsson L et al. Comparison of One- and Two-Day Protocols for Myocardial SPECT: A Monte Carlo Study. *Clin Physiol Func Imaging* 2005; 25: 189-95.
21. Wackers F, Berman D, Maddahi J et al. Technetium-99m Hexakis 2-Methoxyisobutyl Isonitrile: Human Biodistribution, Dosimetry, Safety, and Preliminary Comparison to Thallium-201 for Myocardial Perfusion Imaging. *J Nucl Med* 1989; 30: 301-11.
22. Ljungberg M, Strand SE. A Monte Carlo program for the simulation of scintillation camera characteristics. *Comput Methods Programs Biomed* 1989; 29: 257-72.
23. Fricke E, Fricke H, Weise R et al. Attenuation correction of myocardial SPECT perfusion images with low-dose CT: evaluation of the method by comparison with perfusion PET. *J Nucl Med* 2005; 46: 736-44.
24. Patton JA, Turkington TG. SPECT/CT physical principles and attenuation correction. *J Nucl Med Technol* 2008; 36: 1-10.
25. Turkington TG. Attenuation correction in hybrid positron emission tomography *Semin Nucl Med* 2000; 30: 255-67.
26. Hendel RC, Berman DS, Cullom SJ et al. Multicenter Clinical Trial to Evaluate the Efficacy of Correction for Photon Attenuation and Scatter in SPECT Myocardial Perfusion Imaging. *Circulation* 1999; 99: 2742-9.
27. Ficaro EA, Fessler JA, Shreve PD et al. Simultaneous transmission/emission myocardial perfusion tomography: diagnostic accuracy of attenuation corrected 99mTc-sestamibi single-photon emission computed tomography. *Circulation* 1996; 93: 463-73.
28. Hashimoto J, Kubo A, Ogawa K et al. Scatter and attenuation correction in technetium-99m brain SPECT. *J Nucl Med* 1997; 38: 157-62.
29. Ogawa K, Harata Y, Ichihara T et al. A practical method for position-dependent Compton-scatter correction in single-photon emission CT. *IEEE Trans Med Imaging* 1991; 10: 408-12.
30. Ichihara T, Ogawa K, Motomura N et al. Comptom scatter correction using triple-energy window method for single- and dual-isotope SPECT. *J Nucl Med* 1993; 34: 2216-21.
31. Frey EC, Ju ZW, Tsui BMW. A Fast Projector-Backprojector Pair Modeling the Asymmetric, Spatially Varying Scatter Response Function for Scatter Compensation in SPECT Imaging *IEEE Trans Nucl Sci* 1993; 40: 1192-7.
32. Ichihara T, Motomura N, Ogawa K et al. Evaluation of SPET quantification of simultaneous emission and transmission imaging of the brain using a multi detector SPET system with the TEW scatter compensation method and fan-beam collimation. *Eur J Nucl Med* 1996; 23: 1292-9.
33. Masood Y, Liu YH, Depuey G et al. Clinical validation of SPECT attenuation correction using x-ray computed tomography-derived attenuation maps: multicenter clinical trial with angiographic correlation. *J Nucl Cardiol* 2005; 12: 676-86.
34. Hayashi M, Deguchi J, Utsunomiya K et al. Comparison of methods of attenuation and scatter correction in brain perfusion SPECT. *J Nucl Med Technol* 2005; 33: 224-9.
35. Goetze S, Wahl RL. Prevalence of misregistration between SPECT and CT for attenuation corrected myocardial perfusion SPECT. *J Nucl Cardiol* 2007; 14: 200-6.
36. Goetze S, BrownTL, Lavely WC et al. Attenuation correction in myocardial perfusion SPECT/CT: effects of misregistration and value of reregistration. *J Nucl Med* 2007; 48: 1090-5.